Published in final edited form as:
Nanomedicine (Lond). 2011 June ; 6(4): 715–728. doi:10.2217/nnm.11.19.

Nanoparticle PEGylation for imaging and therapy

Jesse V Jokerst[1], **Tatsiana Lobovkina**[2], **Richard N Zare**[2,3], and **Sanjiv S Gambhir**[†,1,3]

[1]Molecular Imaging Program at Stanford (MIPS), Department of Radiology, 318 Campus Drive, Stanford University, Stanford, CA 94305-5427 USA

[2]Department of Chemistry, Stanford University, 333 Campus Drive, Stanford, CA 94305-5080 USA

[3]Bioengineering, Materials Science & Engineering, Bio-Xc, Stanford University, Stanford, CA 94305, USA

Abstract

Nanoparticles are an essential component in the emerging field of nanomedical imaging and therapy. When deployed *in vivo*, these materials are typically protected from the immune system by polyethylene glycol (PEG). A wide variety of strategies to coat and characterize nanoparticles with PEG has established important trends on PEG size, shape, density, loading level, molecular weight, charge and purification. Strategies to incorporate targeting ligands are also prevalent. This article presents a background to investigators new to stealth nanoparticles, and suggests some key considerations needed prior to designing a nanoparticle PEGylation protocol and characterizing the performance features of the product.

Keywords

circulation time; nanoparticle; PEG; PEG conjugation; PEG length; PEG quantitation; polyethylene glycol

Nanoparticles (NPs) are synthetic materials with dimensions from one to hundreds of nanometers, and remarkable applications in biomedicine due to the unique way in which they interact with matter [1,2]. There are currently more than 35 US FDA-approved NPs often incorporating polyethylene glycol (PEG), with a larger number in preclinical studies for both imaging and therapy (Figure 1A) [1,3–9]. NPs have large payloads, stability, avidity, signal enhancement and the capacity for multiple, simultaneous applications owing to their unique size and high surface area:volume ratio [10]. While they are bigger than molecules and many proteins, yet smaller than cells, they behave differently to other therapies and imaging agents, affecting their *in vivo* applications. For example, in cancer tissue, NPs not only extravasate from the leaky tumor vasculature to a higher degree than healthy tissue, but also remain in the area by the enhanced permeability and retention (EPR) effect [11]. NPs lodged in the tumor can then perform signaling and/or therapy [10].

Despite these advantages, some fundamental challenges hamper NP deployment to the clinic. These include uptake by the reticuloendothelial system (RES), in which NPs are rapidly shuttled out of circulation to the liver, spleen or bone marrow, and nonspecific

[†]Author for correspondence: Tel.: +1 650 725 2309 Fax: +1 650 724 4948 sgambhir@stanford.edu.

The authors have no other relevant affiliations or financial involvement with any organization or entity with a financial interest in or financial conflict with the subject matter or materials discussed in the manuscript apart from those disclosed.

binding of NPs to nontargeted or nondiseased areas. Concerns about NP toxicity often arise because of this RES accumulation. Aggregation can lead to NP entrapment in the liver, lungs or elsewhere due to capillary occlusion [12].

The addition of PEG to the NP surface (PEGylation) can reduce many of these challenges (Figure 1B). PEG is a coiled polymer of repeating ethylene ether units with dynamic conformations (Figure 1C). In both drug-delivery and imaging applications, the addition of PEG to NPs reduces RES uptake and increases circulation time versus uncoated counterparts [13]. Aggregation decreases owing to passivated surfaces, and association with nontargeted serum and tissue proteins is diminished, resulting in so-called `stealth' behavior. The PEG chains reduce the charge-based contact typical of proteins and small-molecule interactions. Solubility in buffer and serum increases due to the hydrophilic ethylene glycol repeats and the EPR effect is modulated due to NP size changes via addition of a PEG coat [14,15]. Due to these attributes, PEGylated NPs generally accumulate in the liver a half to a third of the amount of non-PEGylated NPs and demonstrate higher tumor accumulation versus background [16]. PEG is inexpensive, versatile and FDA approved for many applications [12].

This article summarizes PEG utilization in NP systems. Rather than a comprehensive review, it is an introduction to the many factors that need consideration in a PEGylation protocol. Emphasis will be given to the selection of proper PEG type, methods to quantify the amount of PEG per NP, and the effect these variables have on *in vivo* behavior. Attention is given to NPs deployed for imaging and drug-delivery applications. Excellent reviews on protein and peptide PEGylation exist in the literature [17].

Mechanisms of PEG action

All NPs contain at least two fundamental spatial components: the core and the corona that interact with the environment or solvent. While core/shell, core/multishell systems add further complexity, for example [18], all still possess an area in which NP interfaces with the solvent (Figure 1B). PEG chains modify this interface layer and increase circulation time. Circulation half-time ($t_{½}$) describes blood pool residence and is the period over which the concentration of circulating NPs remains above 50% of the injected dose, analogous to a drug's half-life [19]. NP efficacy requires sufficient $t_{½}$ to not only reach the target, but also remain in the affected area (at concentrations sufficiently above background tissue) long enough for image capture or drug delivery. The RES system prevents site-specific accumulation because it removes the NPs from circulation, acting as a competitor to the intended target site [20]. In addition, the NPs must clear from the non-targeted area to produce imaging contrast or dosing efficiency.

The ideal $t_{½}$ is dependent on application. In imaging, 2–6 h is optimal for injection, accumulation at targeted site, clearance from nontargeted areas and data collection. The ideal circulation time for therapeutic NPs is longer (days) to allow repeated exposure to affected area. Unfortunately, this can also expose healthy organ systems to the drug and is the motivation for targeted NPs, as such systems preferentially accumulate in the diseased area.

Approaches to measuring $t_{½}$ vary with NP type. When labeled with radionuclides, γ counting of either specific organ systems or blood aliquots determines NP circulation time. One limitation is dissociation of radionuclide from NPs; however, radioactivity measurements may always be carried out noninvasively [21]. Measurement of $t_{½}$ via fluorescence, Raman, inductively coupled plasma or chromatography/mass spectrometry is very specific to the NP, but requires sequential sampling of the blood pool.

The RES is an immune system component, utilizing circulating macrophages and monocytes, liver Kupffer cells and spleen and other lymphatic vessels to remove foreign material, such as bacteria and viruses, from the body [20]. Figure 2 illustrates how opsonin proteins associate with foreign bodies and coat its surface [22]. As bacteria and viruses have the same negative surface charge as phagocytic cells, opsonins are critical to reducing the charge repulsion between the two systems [13]. Next, phagocytic cells engulf the material and transport it to the liver or spleen for degradation and excretion (Figure 2 A3–A4). Additional phagocytic macrophages are permanently located in the liver. Known as Kupffer cells, these cells serve as a major filter for many types of NPs and are a major interference with long $t_{½}$ [23]. The PEG polymer on a NP surface increases $t_{½}$ by reducing this opsonization process (Figure 2B2), thus preventing recognition by monocytes and macrophages, allowing the NPs to remain in the blood pool [13,22]. Hydrophobic particles are also more vulnerable to the RES and hydrophilic PEG reduces these complications [22].

In addition to NP–RES interactions, poor $t_{½}$ can also result from NP–NP interactions (i.e., aggregation). NPs aggregate primarily because the attraction between particles is stronger than the attraction for solvent [13,24]. NPs with a high surface energy have a greater tendency to aggregate as described by the Derjaguin-Landau-Verwey-Overbeek (DLVO) theory [25,26]. For spherical NPs, the interaction potential is related to the electrostatic repulsive potential and the van der Waals attraction potential [26]. PEG decreases the surface energy of NPs and minimizes van der Waals attraction [27–29].

Aggregation can be induced by solvents of high (>100 mM) ionic strength (shielding of solvent from NP), highly concentrated solutions of NPs (less distance between the NPs), time from synthesis, or NP preparations with a very neutral (~±5 mV) zeta potential [30]. PEG decreases the amount of attraction between NPs by increasing the steric distance between them and increasing hydrophilicity via ether repeats forming hydrogen bonds with solvent. Other benefits to PEGylation include modifying the size of the particle. The reduced renal filtration of particles larger than 10 nm increases $t_{½}$; however, at too large a size (>100 nm), liver uptake increases and EPR extravasation may decrease [31]. PEG modifies the NP flexibility and the NP can become `softer' after PEGylation than the underlying material, influencing extravasation.

PEG applications

Prior to NP applications, PEG was used as a nontoxic, water-soluble dispersant/stabilizer. Also known as Carboxwax®, it is present in health and beauty aids, including laxatives, toothpastes and eye drops, and is an excipient in tablet formulations [32]. PEG stabilizes organ and blood donations.

Early work with PEGylated NPs stemmed mostly from drug delivery [16,33–36]. One of the first reports on PEGylation was described by Davis and Abuchowski [37,38], where they covalently attached methoxy-PEGs (mPEGs) of 1900 and 5000 Da to bovine serum albumin and to liver catalase. Later, acrylic microspheres functionalized with PEG-modified human serum albumin increased $t_{½}$ *in vivo* [39]. Li and colleagues found that 75-nm latex particles remained in rat circulation 40-times longer (half-life 20 min vs 13 h) when coated than uncoated with PEG larger than 5000 kDa [33]. Klibanov and Huang found that incorporation of dioleoyl *N*-(monomethoxy polyethyleneglycol succinyl) phosphotidylethanolamine (PEG-PE) into posphatidylcholine:cholesterol liposomes (1:1) increased $t_{½}$ from 30 min to 5 h without increasing leakage of the liposome interior [35]. In the mid-1990s, Doxil® (liposomal delivery vehicle for doxorubicin) and oncospar (PEG-L-asparaginase) became the first FDA-approved NP therapeutics [40]. Doxil increases doxorubicin bioavailability nearly 90-fold at 1 week from injection of PEGylated liposomes

versus free drug [41]. The use of PEG on the doxorubicin carrier yields a drug half-life of 72 h with circulation half-life of 36 h [42,43]. Later, Abraxane® was introduced as an albumin-functionalized NP for delivery of taxane without cremphor to enhance drug efficiency [44].

Considerations on PEGylation

The PEG monomer and the basic structure of the polymer are shown in Figure 1C. Most PEG molecules contain the following components: one end (designated R_1) attaches to the NP surface, while the other distal terminal group (R_2) interacts with the solvent. Any number (n) of ethylene glycol repeats connect R_1 and R_2. PEG is also described as polyethylene oxide, especially when referring to longer PEG repeats or mPEG [45]. Below the major factors affecting the behavior of PEG–NP constructs are considered, in light of increased $t_{½}$.

NP type

The type of NP to be PEGylated remains the most important factor for stability and $t_{½}$. It is most affected by the NP size, charge and composition. For example, ganglioside liposomes have a size-dependent distribution (<70 nm accumulate in liver and >200 nm in spleen), while identical liposomes of phosphatidylserine showed size-independent liver accumulation [46]. In the case of NPs with positive surface charges and sizes above 100 nm, the NPs are still rapidly cleared from the circulation in the face of even the most careful PEGylation strategies [31,47]. PEG types appropriate for a liposome NP may fail when deployed to solid, metallic NPs as liposomal NPs better mimic naturally circulating entities (i.e., cells) and, thus, may not require as stringent of a PEGylation protocol. NP composition is the most important consideration when selecting a PEG conjugation approach.

In imaging, one of the first NP applications was superparamagnetic iron oxide (SPIO) and reports of this material in nanomaterial form date from the 1960s [48,49] and had become routine by the 1990s [50]. PEGylation or dextran coating of SPIO and ultrasmall SPIO (USPIO) lengthens $t_{½}$ by up to 200 min and improves image quality [51–53]. Targeted SPIO allows molecular imaging via MRI, generally impossible without exogenous contrast agents [54]. Gold NPs were first used as immunogold for transmission electron microscopy contrast in the 1970s, but are now also used for computed tomography and radiograph contrast [55,56]. Many applications of PEGylated gold NPs and nanorods have since been reported [57–62]. A fundamental challenge of gold NPs for CT is low sensitivity. High amounts are needed to achieve contrast. Silica NPs have applications in MRI as gadolinium containers or to protect inner imaging cores [63,64]. NPs deployed to molecular imaging include quantum dots (QDs) for optical reporting [65–67], carbon nanotubes and gold nanorods for photoacoustic imaging and gold surface-enhanced Raman scattering NPs [68–70]. Both QDs and carbon nanotubes suffer from toxicity concerns [71]. Some NPs are multimodal – that is, they report signal through more than one method (e.g., fluorescence and MRI) [72,73].

In therapeutic applications, the NP scaffold stabilizes the payload (~10^4–10^5 copies of drug molecules per NP [74,75]), allowing a metered release of drug, reducing toxicity and side effects, and increasing patient compliance [31]. Hydrophobic drugs are protected by the NP interior [15]. Rather than the solid metallic NPs used in imaging, most therapeutic drug-carrying NPs are in the form of liposomes or lipid-based complexes, as well as polymeric micelles or biodegradable polymer/drug composites [76–78]. One of the most common substrate is a blend of poly(lactic-co-glycolic acid) (PLGA) and PEG, (PLGA–PEG). However, there are many other PEGylated polymers for making drug-containing NPs, including polylactic acid [79], poly(hexadecylcyanoacrylate) (PHDCA) [21], polycaprolactone [80], chitosan [81] and poly(sebacic acid) [82]. RNA interference (RNAi) via NPs or PEGylated cationic polymers and lipids are reported [3,5,83,84]. Metallic NPs

are also used in tandem with infrared heating for therapy; nanoshells and nanorods are the most common examples [85]. Other NP types detailed in Table 1 include silica, phosphors ($NaYF_4$) and QDs [86,87].

Length & conformation of PEG chain

Larger PEG chains contain more monomer repeats, n, (Table 1). Although some reports list the number of monomers in the polymer (e.g., PEG_{40} would be 40 ethylene glycol repeats), the most common way of reporting the size/length of the PEG chain is the molecular weight, with the weight average molar mass (M_w) being the most common [88]. Some common PEG M_w values include 2000, 3400, 5000, 10,000 and 20,000 Da (i.e., PEG_{20K}). The M_w of a given PEG can be roughly translated into n monomers by dividing M_w by 44, which is the approximate molecular weight of one ethylene glycol monomer moiety or residue.

Larger PEG chains ($n = 10^3–10^4$) are bigger molecules, and the thickness of a grafted PEG layer on the NP surface correlates with polymer conformation. Polymer conformation can be described in terms of the Flory radius (F) according to Equation 1, where n is the number of monomers per polymer chain and α is the length of one monomer in Angstroms (α = 3.5 Å for PEG) [89,90]. The F of some typical PEG M_w are plotted in Figure 3B. There are two main conformations that PEG chains can acquire depending on grafting density. If the surface density is low (i.e., the distance D, between the attachment points of polymer to a surface is larger than F), polymer chains will acquire a `mushroom' conformation (Figure 4A). In this conformation, a polymer chain occupies roughly a half sphere with a radius comparable to the Flory radius. For increased grafting densities (D < F), a polymer will acquire a `brush' regime, with long, thin bristles of PEG extending from the NP surface (Figure 4B) [89,90]. The number of repeating units required to transition from mushroom to brush arrangement is highly dependent on the type of PEG and NP [91]. Pastor and coworkers report that mushroom conformation becomes brush-like when the distance between individual PEG molecules on the surface nears F [45]. NPs with brush PEG generally have longer circulation times as the denser coatings better shield the NPs from the RES [92]. These two different PEG orientations illustrate the wide diversity in PEG footprints in Table 1 and explain footprints smaller than F detailed in Table 2. The PEG footprint in Table 2 is the average space occupied by one PEG on the surface and is not related to F. It is the effective distance between graft sites and is determined by dividing NP surface area by number of PEG ligands. When only the distal R_1 occupies NP area, the footprint may be smaller than F.

$$F = \alpha n^{\frac{3}{5}} \quad (1)$$

In general, smaller therapeutic materials use larger PEGs [17]. Oligos and small molecules may be coated with PEG 20,000–50,000 to prevent excretion by the kidneys and maintain a high blood pool concentration for longer periods of time (by enhancing recirculation). Larger NPs in the 50–100-nm range are frequently coated with smaller lengths of PEG (3400–10,000) because further increases in hydrodynamic radius could shorten $t_{½}$ [12]. Kidney excretion of unconjugated PEG decreases as a function of molecular weight, but liver uptake increases [12]. Mori and Huang, in 1991, reported that liposome circulation time with PEG_{5000} is significantly longer (7 h) than PEG_{2000} or PEG_{750} (~1 h) [93]. Some reports indicate that larger M_w PEGs produce longer $t_{½}$ on QDs [94–96]. The larger a PEG, the fewer copy numbers can be loaded onto a NP in mushroom conformation.

Important exceptions to the general structure shown in Figure 1C include star PEG, branch PEG and comb PEG [97]. Branch PEGs have one to three pendent PEG units deviating from

a central backbone annealed to the NP surface, while star PEGs have several branches emanating from a central point. Branch PEGs result in carbon nanotubes with $t_{½}$ values of 21 h [98]. NPs with blended PEG chains (two different PEG types on the same NP) are also common and typically involve a high-density short PEG (M_w = 2 kDa) for stealth and a lower density, longer (M_w = 5 kDa; ratio 1:5) PEG for attaching targeting ligands and preventing loop formation in the longer components [99].

PEG terminus

The terminal end of the polymer indicated as R_2 in Figure 1C influences *in vivo* behavior. Whitesides compared PEG with different terminal groups and identified that a PEG methoxy or alcohol terminus reduced nonspecific binding of the model proteins lysosyme and fibrinogen to self-assembled monolayers of alkane thiol repeats by orders of magnitude compared with non-PEGylated or alternative terminus [100,101]. mPEG is so ubiquitous that it is often implied when an investigator mentions PEG. Nevertheless, a broad range of PEG types are commercially available, including halo, azido, sulfo and thiol derivatives [102].

As the cell surface is negative, coating NPs with a negative charge (thiol or carboxyl) causes fewer phagocytotic events than positive charges (amine) [31]. Others have studied simple hydroxyl for reducing nonspecific binding [103]. Termini other than methoxy are most commonly used to localize a succimide-, maleimide- or alkyne-reactive group on the end of the PEG to facilitate later binding of a secondary targeting ligand via amine, thiol or click chemistry, respectively [104]. One problem is steric crowding. At coating densities below the brush threshold, the reactive site can sometimes be hidden deep inside the mushroom coil, which prevents secondary linkage (see `Ligands' section).

Linkage to NP

After selection of the proper PEG, the next consideration is annealing it to the NP surface. Both covalent and noncovalent approaches are used. For solid NPs, such as gold, thiol binding is the classic approach where a sulfhydryl-capped PEG chain adheres to the gold surface [105]. To increase stability, the Mattoussi group and others have deployed multidentate ligands (e.g., dihydrolipoic acid) for more robust PEG stabilization than simple thiols [106]. Silica NP surfaces are generally capped with an organosilane such as amino- or mercapto-trimethoxysilane for routine bioconjugation [104].

A commonly used approach for noncovalent PEGylation is coating the hydrophobic NP surface with lipid-PEG conjugates. For example, PEGylated phospholipids with linear or branched PEG chains bind to the hydrophobic surface of single-walled carbon nanotubes in such a way that hydrophilic PEG groups are facing the aqueous exterior and provide the nanotubes with hydrophilic PEG corona [107,108]. Other techniques prepare hydrophobic polymeric NPs [109], oleic acid-coated magnetic NPs [110] or QDs [111] coated with PEGylated lipids. The hydrophobic interactions between lipids and NPs anchor the PEG chain. For the liposomal preparations, it is also feasible to simply include PEGylated lipids into the lipid mixture [112], or incubate non-PEGylated lipid nanopcapsules with aqueous micellar solution of PEGylated lipids [113]. Regardless of immobilization chemistry, purification of the PEG-NP conjugate is carried out via repeated centrifugation and washing steps, filtration, dialysis or by separation methods, such as size-exclusion or ion-exchange chromatography.

Characterization methods

Dynamic light scattering offers three important characteristics of the final PEGylated NP: NP size, zeta potential and size distribution [114]. The zeta descriptor measures the

electrostatic potential that exists between the shear plane of a NP and the solvent, and provides information on the colloidal stability of the NP. It is dependent on the solvent, salt type and concentration, and pH. High charge differences (>±10 mV) lead to greater interparticle repulsion. The zeta potential also offers information on the surface coating. Thiols and carboxyls have negative values while amines have positive charge. Sizing via dynamic light scattering suffers from poor reproducibility, yet it is quick and can be used to monitor the sequential size increases that occur during PEGylation and bioconjugation. The size distribution can be used to measure the homogeneity of the final product. Although size increases offer evidence for NP PEGylation and may discriminate between brush and mushroom PEG configurations [115], it cannot answer the specific loading level (i.e., the number of PEG units bound per NP).

Unfortunately, this measurement is only studied casually with many reports simply using NP surface area, PEG size and an assumption of complete saturation to determine loading levels. Another suboptimal alternative is to measure the PEG concentration before and after incubation with the NPs, remove the NPs by filtration or centrifugation and suggest that the difference in solution-phase PEG is immobilized on the NPs. While many of the PEGs are attached, a large number are also nonspecifically bound. This technique often overestimates the loading level by orders of magnitude and is especially difficult when large excess of PEG is used as the measurement of slight differences.

Different types of analytical chemistry solutions for measuring the PEG:NP ratio are detailed in Table 2, and report three different metrics for PEG loading levels (PEG:NP ratio, pmol of PEG/cm^2 and PEG footprint) [116]. While footprints (the area of NP surface occupied by each PEG molecule) smaller than F may be counterintuitive, the very dense brush coatings created result in the small footprint and describe a situation in which only the terminal end of the PEG occupies space on the NP surface. While Raman analysis offers very detailed information on loading and conformation, it is beyond the scope of routine laboratories [91]. Thermogravimetric analysis measures change in weight as a function of temperature increase (PEG loss) and is reported for this purpose, but also requires specialized equipment [117]. For the routine user, NMR is used to detect the ethylene protons at 3.65 parts per million, but is not quantitative [118,119]. We, and others, have successfully used fluorescent analogs of the PEG to model the binding densities possible at different loading levels [120,121]. This approach may not be appropriate for gold NPs because of quenching. Other possible methods include surface plasmon resonance (mostly for flat surfaces), size-exclusion chromatography, gels and colorimetric approaches that utilize a reactive R_2 [116,122,123]. Gas or liquid chromatography could also be used to not only remove loosely bound PEG, but also offer indirect quantitative information on the NP's PEG loading [124].

Perhaps the most important characterization metric is $t_{½}$, which is measured by injecting a known amount of NPs into an animal subject and serially collecting blood to monitor the amount of NP in circulation. Approaches to measuring the NP concentration include γ counting, elemental analysis, and mass spectrometry. Some representative $t_{½}$ values for PEGylated nanomaterials are presented in Table 3. With the proper matching of PEG to NP, long $t_{½}$ values are achieved. Circulation times near 120 h have been reported for PEGylated xyotax (paclitaxel encapsulated in a biodegradable polyglutamate polymer; also known as OPAXIO) in humans [77,125].

Ligands

The ideal PEG R_2 reduces nonspecific protein absorption, increases hydrophilicity, prevents NP aggregation and facilitates ligand binding for targeted NPs. Compared with the passive targeting via the EPR effect, targeted NPs combine a recognition element with the

PEGylated particle for increased accumulation at the site of interest [126–128]. Ligands can increase the tumor accumulation caused by the EPR effect and targeted NPs offer site-specific accumulation, followed by release of a therapeutic not restricted to the vasculature. Ligand types include antibodies [129], small peptides or molecules [128,130–132], lectins [133], aptamers [134], engineered proteins [135] and protein fragments [136]. As NPs leave the vasculature to a lesser degree than small molecules, they are especially useful for targeting markers of angiogenesis [131]. Recent work has shown NPs to be effective vehicles of RNAi outside the vasculature [5]. Both the VEGF and $\alpha_v\beta_3$ integrins have been imaged via PEGylated NPs to assess tumor vascularization [137]. Without PEGylation, the NPs would have decreased opportunity to interface with vascular targets. Importantly, the use of such ligands (while increasing NP specificity), can also come at the expense of NP performance. As these targeting molecules have exposed charged regions, they can compromise the integrity of the stealth coat and increase RES uptake. The mPEGs, which offer the least nonspecific binding, have no bioconjugation activity, and must be modified or replaced with less stealthy options.

One solution is to use PEGs with reactive ends, although this may increase nonspecific binding (Figure 5A & Table 4). Another approach is blended PEGs, in which one type offers stealth character, while another offers binding capacity [99]. A further option is to anneal the ligand to the NP surface via the same surface reactive sites as the PEG molecules, and coat the remaining sites with PEG, as shown in Figure 5B [138]. One challenge of this approach is steric hindrance of the ligand binding sites by PEG. An additional challenge is quantifying the number of ligands present on the NP, which is important for avidity amplification measurements. Similar approaches to PEG quantification are used; however, since ligands generally have more reactive sites than PEG they can be fluorescently tagged and this reporter used for ligand:NP ratios for all NPs except those that quench fluorescence (i.e., gold NPs).

Targeting of some lipid-based nanocarriers can also be achieved by inserting peptide-lipid conjugates into the outer layer of a parent PEGylated liposome [139]. Alternatively, receptor-targeted nanocomplexes can be prepared by mixing PEGylated cationic liposomes with peptide and drug (plasmid DNA) at precise mixing ratios [140]. Using a mixture of PEGylated, non-PEGylated polymers, as well as polymer–PEG–ligand conjugates during NP preparation, allows for single-step surface functionalization of polymeric NPs [141].

Complications, alternatives & future perspective

Despite these achievements, a number of limitations and challenges still hamper complete deployment of PEG [12]. Although PEG toxicity is low, it does occur with frequency inversely proportional to molecular weight, especially after oral ingestion. Toxicity after intravenous injection is more likely owing to the NP than the PEG corona. Immunogenicity has also been reported, but generally less so than the immunogenicity of the NP [142]. Furthermore, repeated injections of PEGylated material show markedly decreased $t_{½}$. This `accelerated blood clearance' (or ABC effect), is thought to be a result of increased splenic production of IgM [143]. While the resistance of PEG to serum degradation is useful from a stability standpoint, NPs and coatings that safely biodegrade *in vivo* after a defined time point are desirable. A final challenge of PEG is degradation by light, heat or sheer stress, which can result in fragmentation of the PEG and diminish cloaking ability [12].

Alternatives to PEG include natural products, PEG hybrids, and next-generation polymers. Chitons, dextran and other saccharide-containing products have been used to deliver doxorubicin [144,145]. PLGA/PEG copolymer, and polyvinyl pyrrolidone have also shown promise at maintaining long $t_{½}$ [146,147]. Dendrimers offer both a scaffold for NP synthesis and also a stabilizing sheath [148]. Poly amino acids have a biodegradable structure, but less

stealth capacity. Coatings and NPs that better mimic the body's innate stealthing of circulating materials, such as lipids, are increasingly reported [149]. These particles may offer even better shielding and can have site-selective biodegradation. Other researchers report micelles and liposomes that detach the PEG coat to facilitate endosomal escape upon entering the cell [150,151]. Alternatively, cell or bacteria have been deployed as a `Trojan Horse' to deliver NPs [152,153]. Additional NPs are responsive to pH as tumors are usually acidic relative to the rest of the body (pH ~7.4) [154,155]. Langer and others have designed NPs from a triblock copolymer of poly(ethylene oxide) and poly(propylene oxide) and poly(β-amino ester), which degrade and release their therapeutic payload at pH less than 6.5 [156].

Conclusion

The use of PEG and similar stabilizers on NP surfaces will undoubtedly continue. It is unclear how emerging materials will complement PEG's role as the gold-standard cloaking agent. NPs that transition from passive targeting via the EPR effect to NPs that are truly selective for a molecular phenotype will likely require PEG or equivalent to promote circulation time and inhibit removal by the liver and spleen. Strategies to combine the signaling or therapeutic benefits of NPs with effective *in vivo* delivery remain one of the primary challenges in nanomedicine.

Acknowledgments

Financial & competing interests disclosure This work was supported by funding from NCI ICMIC P50CA114747 (SSG), NCI CCNE-T U54 U54CA151459, NIBIB BRP 5-RO1-EBB000312 (SSG), NCI U01 EDRN CA152737, Doris Duke Foundation, Canary Foundation, Ben and Catherine Ivy Foundation, Sir Peter Michael Foundation. JV Jokerst is grateful for SMIS fellowship support (R25 CA118681). RN Zare and T Lobovkina acknowledge the National Science Foundation under CBET-0827806. T Lobovkina is the recipient of the Knut and Alice Wallenberg Foundation, Sweden.

No writing assistance was utilized in the production of this manuscript.

Bibliography

1. Wagner V, Dullaart A, Bock A, Zweck A. The emerging nanomedicine landscape. Nat. Biotechnol. 2006; 24(10):1211–1218. [PubMed: 17033654]
2. Kim BY, Rutka JT, Chan WC. Nanomedicine. N. Eng. J. Med. 2010; 363(25):2434–2443.
3. Jacobson GB, Gonzalez-Gonzalez E, Spitler R, et al. Biodegradable nanoparticles with sustained release of functional siRNA in skin. J. Pharm. Sci. 2010; 99(10):4261–4266. [PubMed: 20737633]
4. O'Brien ME, Wigler N, Inbar M, et al. Reduced cardiotoxicity and comparable efficacy in a Phase III trial of pegylated liposomal doxorubicin HCl (CAELYX/doxil) versus conventional doxorubicin for first-line treatment of metastatic breast cancer. Ann. Oncol. 2004; 15(3):440–449. [PubMed: 14998846]
5. Davis ME, Zuckerman JE, Choi CH, et al. Evidence of RNAi in humans from systemically administered siRNA via targeted nanoparticles. Nature. 2010; 464(7291):1067–1070. [PubMed: 20305636]
6. Scranton R, Cincotta A. Bromocriptine – unique formulation of a dopamine agonist for the treatment of Type 2 diabetes. Expert Opin. Pharmacother. 2010; 11(2):269–279. [PubMed: 20030567]
7. Lim WT, Tan EH, Toh CK, et al. Phase I pharmacokinetic study of a weekly liposomal paclitaxel formulation (Genexol-PM) in patients with solid tumors. Ann. Oncol. 2009; 21(2):382–388. [PubMed: 19633055]
8. Winter PM, Morawski AM, Caruthers SD, et al. Molecular imaging of angiogenesis in early-stage atherosclerosis with $\alpha_v\beta_3$-integrin-targeted nanoparticles. Circulation. 2003; 108(18):2270–2274. [PubMed: 14557370]

9. Keren S, Zavaleta C, Cheng Z, et al. Noninvasive molecular imaging of small living subjects using Raman spectroscopy. Proc. Natl Acad. Sci. USA. 2008; 105(15):5844–5849. [PubMed: 18378895]
10. Jain PK, Huang X, El-Sayed IH, El-Sayed MA. Noble metals on the nanoscale: optical and photothermal properties and some applications in imaging, sensing, biology, and medicine. Acc. Chem. Res. 2008; 41(12):1578–1586. [PubMed: 18447366]
11. Maeda H, Wu J, Sawa T, Matsumura Y, Hori K. Tumor vascular permeability and the EPR effect in macromolecular therapeutics: a review. J. Control Release. 2000; 65(1–2):271–284. [PubMed: 10699287]
12. Knop K, Hoogenboom R, Fischer D, Schubert US. Poly(ethylene glycol) in drug delivery: pros and cons as well as potential alternatives. Angew Chem. Int. Ed. Engl. 2006; 49(36):6288–6308. [PubMed: 20648499]
13. van Vlerken LE, Vyas TK, Amiji MM. Poly(ethylene glycol)-modified nanocarriers for tumor-targeted and intracellular delivery. Pharm. Res. 2007; 24(8):1405–1414. [PubMed: 17393074]
14. Kanaras AG, Kamounah FS, Schaumburg K, Kiely CJ, Brust M. Thioalkylated tetraethylene glycol: a new ligand for water soluble monolayer protected gold clusters. Chem. Commun. 2002; 20:2294–2295.
15. Kwon GS. Polymeric micelles for delivery of poorly water-soluble compounds. Crit. Rev. Ther. Drug Carrier Syst. 2003; 20(5):357–403. [PubMed: 14959789]
16. Gref R, Minamitake Y, Peracchia MT, et al. Biodegradable long-circulating polymeric nanospheres. Science. 1994; 263(5153):1600–1603. [PubMed: 8128245]
17. Roberts MJ, Bentley MD, Harris JM. Chemistry for peptide and protein PEGylation. Adv. Drug Deliv. Rev. 2002; 54(4):459–476. [PubMed: 12052709]
18. Li D, He Q, Li J. Smart core/shell nanocomposites: intelligent polymers modified gold nanoparticles. Adv. Colloid Interface Sci. 2009; 149(1–2):28–38. [PubMed: 19201389]
19. Prencipe G, Tabakman SM, Welsher K, et al. PEG branched polymer for functionalization of nanomaterials with ultralong blood circulation. J. Am. Chem. Soc. 2009; 131(13):4783–4787. [PubMed: 19173646]
20. Saba TM. Physiology and physiopathology of the reticuloendothelial system. Arch. Intern. Med. 1970; 126(6):1031–1052. [PubMed: 4921754]
21. Peracchia MT, Fattal E, Desmaële D, et al. Stealth PEGylated polycyanoacrylate nanoparticles for intravenous administration and splenic targeting. J. Control. Release. 1999; 60(1):121–128. [PubMed: 10370176]
22. Owens D 3rd, Peppas N. Opsonization, biodistribution, and pharmacokinetics of polymeric nanoparticles. Int. J. Pharmaceut. 2006; 307(1):93–102.
23. Decker K. Biologically active products of stimulated liver macrophages (Kupffer cells). Eur. J. Biochem. 1990; 192(2):245–261. [PubMed: 2170121]
24. Zolnik BS, Sadrieh N. Regulatory perspective on the importance of ADME assessment of nanoscale material containing drugs. Adv. Drug Deliv. Rev. 2009; 61(6):422–427. [PubMed: 19389437]
25. Guzman K, Finnegan M, Banfield J. Influence of surface potential on aggregation and transport of titania nanoparticles. Environ. Sci. Technol. 2006; 40(24):7688–7693. [PubMed: 17256514]
26. Yang P, Ando M, Murase N. Various Au nanoparticle organizations fabricated through SiO_2 monomer induced self-assembly. Langmuir. 2010; 27(3):895–901. [PubMed: 21188967]
27. Jun Y, Casula M, Sim J, et al. Surfactant-assisted elimination of a high energy facet as a means of controlling the shapes of TiO_2 nanocrystals. J. Am. Chem. Soc. 2003; 125(51):15981–15985. [PubMed: 14677990]
28. Förster S, Antonietti M. Amphiphilic block copolymers in structure-controlled nanomaterial hybrids. Adv. Mat. 1998; 10(3):195–217.
29. Zhao W, Brook M, Li Y. Design of gold nanoparticle based colorimetric biosensing assays. ChemBioChem. 2008; 9(15):2363–2371. [PubMed: 18821551]
30. Sze A, Erickson D, Ren L, Li D. Zeta-potential measurement using the Smoluchowski equation and the slope of the current–time relationship in electroosmotic flow. J. Colloid Interface Sci. 2003; 261(2):402–410. [PubMed: 16256549]

31. Alexis F, Pridgen E, Molnar LK, Farokhzad OC. Factors affecting the clearance and biodistribution of polymeric nanoparticles. Mol. Pharm. 2008; 5(4):505–515. [PubMed: 18672949]
32. Strickley RG. Solubilizing excipients in oral and injectable formulations. Pharm. Res. 2004; 21(2): 201–230. [PubMed: 15032302]
33. Tan JS, Butterfield DE, Voycheck CL, Caldwell KD, Li JT. Surface modification of nanoparticles by PEO/PPO block copolymers to minimize interactions with blood components and prolong blood circulation in rats. Biomaterials. 1993; 14(11):823–833. [PubMed: 8218736]
34. Mueller BG, Kissel T. Camouflage nanospheres: a new approach to bypassing phagocytic blood clearance by surface modified particulate carriers. Pharmaceut. Pharmacol. Lett. 1993; 3(2):67–70.
35. Klibanov AL, Maruyama K, Torchilin VP, Huang L. Amphipathic polyethyleneglycols effectively prolong the circulation time of liposomes. FEBS Lett. 1990; 268(1):235–237. [PubMed: 2384160]
36. Kataoka K, Harada A, Nagasaki Y. Block copolymer micelles for drug delivery: design, characterization and biological significance. Adv. Drug Deliv. Rev. 2001; 47(1):113–131. [PubMed: 11251249]
37. Abuchowski A, McCoy JR, Palczuk NC, Vanes T, Davis FF. Effect of covalent attachment of polyethylene-glycol on immunogenicity and circulating life of bovine liver catalase. J. Biol. Chem. 1977; 252(11):3582–3586. [PubMed: 16907]
38. Abuchowski A, Vanes T, Palczuk NC, Davis FF. Alteration of immunological properties of bovine serum-albumin by covalent attachment of polyethylene-glycol. J. Biol. Chem. 1977; 252(11): 3578–3581. [PubMed: 405385]
39. Arturson P, Laakso T, Edman P. Acrylic microspheres *in vivo*. Blood elimination kinetics and organ distribution of microparticles with different surface characteristics. J. Pharm. Sci. 1983; 72(12):1415–1420. [PubMed: 6663478]
40. Petros RA, DeSimone JM. Strategies in the design of nanoparticles for therapeutic applications. Nat. Rev. Drug Discov. 1999; 9(8):615–627. [PubMed: 20616808]
41. Laginha KM, Verwoert S, Charrois GJ, Allen TM. Determination of doxorubicin levels in whole tumor and tumor nuclei in murine breast cancer tumors. Clin. Cancer Res. 2005; 11(19):6944–6949. [PubMed: 16203786]
42. Ahmed M, Lukyanov AN, Torchilin V, et al. Combined radiofrequency ablation and adjuvant liposomal chemotherapy: effect of chemotherapeutic agent, nanoparticle size, and circulation time. J. Vasc. Interv. Radiol. 2005; 16(10):1365–1371. [PubMed: 16221908]
43. Gabizon A, Shmeeda H, Barenholz Y. Pharmacokinetics of PEGylated liposomal Doxorubicin: review of animal and human studies. Clin. Pharmacokinet. 2003; 42(5):419–436. [PubMed: 12739982]
44. Moreno-Aspitia A, Perez EA. Nanoparticle albumin-bound paclitaxel (ABI-007): a newer taxane alternative in breast cancer. Future Oncol. 2005; 1(6):755–762. [PubMed: 16556053]
45. Lee H, de Vries AH, Marrink SJ, Pastor RW. A coarse-grained model for polyethylene oxide and polyethylene glycol: conformation and hydrodynamics. J. Phys. Chem. B. 2009; 113(40):13186–13194. [PubMed: 19754083]
46. Liu D, Mori A, Huang L. Role of liposome size and RES blockade in controlling biodistribution and tumor uptake of GM1-containing liposomes. Biochim. Biophys Acta. 1992; 1104(1):95–101. [PubMed: 1550858]
47. Ishida O, Maruyama K, Sasaki K, Iwatsuru M. Size-dependent extravasation and interstitial localization of polyethyleneglycol liposomes in solid tumor-bearing mice. Int. J. Pharm. 1999; 190(1):49–56. [PubMed: 10528096]
48. Gallagher PK, Kurkjian CR. The thermal decomposition of some complex oxalates of iron-(III) using the Moessbauer effect. Inorganic Chem. 1966; 5(2):214–219.
49. Anderson JC, Donovan B. Internal ferromagnetic resonance in magnetite. Proc. Phys. Soc. Lond. 1960; 75:149–151.
50. Weissleder R, Elizondo G, Wittenberg J, et al. Ultrasmall superparamagnetic iron oxide: characterization of a new class of contrast agents for MR imaging. Radiology. 1990; 175(2):489–493. [PubMed: 2326474]

51. Gupta AK, Gupta M. Synthesis and surface engineering of iron oxide nanoparticles for biomedical applications. Biomaterials. 2005; 26(18):3995–4021. [PubMed: 15626447]
52. Schmitz S, Taupitz M, Wagner S, et al. Magnetic resonance imaging of atherosclerotic plaques using superparamagnetic iron oxide particles. J. Magn. Reson. Imag. 2001; 14(4):355–361.
53. Xie J, Xu C, Kohler N, Hou Y, Sun S. Controlled PEGylation of monodisperse Fe_3O_4 nanoparticles for reduced non-specific uptake by macrophage cells. Adv. Mat. 2007; 19(20):3163–3166.
54. Artemov D, Mori N, Okollie B, Bhujwalla Z. MR molecular imaging of the Her 2/neu receptor in breast cancer cells using targeted iron oxide nanoparticles. Magn. Reson. Med. 2003; 49(3):403–408. [PubMed: 12594741]
55. Geso M. Gold nanoparticles: a new x-ray contrast agent. Br. J. Radiol. 2007; 80(949):64–65. author reply 65. [PubMed: 17267474]
56. Faulk WP, Taylor GM. An immunocolloid method for the electron microscope. Immunochemistry. 1971; 8(11):1081–1083. [PubMed: 4110101]
57. Wuelfing WP, Gross SM, Miles DT, Murray RW. Nanometer gold clusters protected by surface-bound monolayers of thiolated poly(ethylene glycol) polymer electrolyte. J. Am. Chem. Soc. 1998; 120(48):12696–12697.
58. Mayer ABR, Mark JE. Colloidal gold nanoparticles protected by water-soluble homopolymers and random copolymers. Eur. Polymer J. 1998; 34(1):103–108.
59. Moller M, Spatz JP, Roescher A, et al. Mineralization of gold in block copolymer micelles. Macromol. Symp. 1997; 117:207–218.
60. Spatz JP, Roescher A, Moeller M. Gold nanoparticles in micellar poly(styrene)-b-poly(ethylene oxide) films. Size and interparticle distance control in monoparticulate films. Adv. Mater. (Weinheim, Ger.). 1996; 8(4):337–340.
61. Fathalla M, Li SC, Diebold U, Alb A, Jayawickramarajah J. Water-soluble nanorods self-assembled via pristine C60 and porphyrin moieties. Chem. Commun. (Camb.). 2009; 28:4209–4211. [PubMed: 19585023]
62. von Maltzahn G, Park JH, Agrawal A, et al. Computationally guided photothermal tumor therapy using long-circulating gold nanorod antennas. Cancer Res. 2009; 69(9):3892–3900. [PubMed: 19366797]
63. He X, Nie H, Wang K, et al. *In vivo* study of biodistribution and urinary excretion of surface-modified silica nanoparticles. Anal. Chem. 2008; 80(24):9597–9603. [PubMed: 19007246]
64. Yoon TJ, Yu KN, Kim E, et al. Specific targeting, cell sorting, and bioimaging with smart magnetic silica core-shell nanomaterials. Small. 2006; 2(2):209–215. [PubMed: 17193022]
65. Michalet X, Pinaud FF, Bentolila LA, et al. Quantum dots for live cells, *in vivo* imaging, and diagnostics. Science. 2005; 307(5709):538–544. [PubMed: 15681376]
66. Bentolila LA, Ebenstein Y, Weiss S. Quantum dots for *in vivo* small-animal imaging. J. Nucl. Med. 2009; 50(4):493–496. [PubMed: 19289434]
67. van Schooneveld MM, Vucic E, Koole R, et al. Improved biocompatibility and pharmacokinetics of silica nanoparticles by means of a lipid coating: a multimodality investigation. Nano Lett. 2008; 8(8):2517–2525. [PubMed: 18624389]
68. Qian X, Peng XH, Ansari DO, et al. *In vivo* tumor targeting and spectroscopic detection with surface-enhanced Raman nanoparticle tags. Nat. Biotechnol. 2008; 26(1):83–90. [PubMed: 18157119]
69. De la Zerda A, Zavaleta C, Keren S, et al. Carbon nanotubes as photoacoustic molecular imaging agents in living mice. Nat. Nanotechnol. 2008; 3(9):557–562. [PubMed: 18772918]
70. Zhang Y, Hong H, Cai W. Imaging with Raman spectroscopy. Curr. Pharm. Biotechnol. 2001; 11(6):654–661. [PubMed: 20497112]
71. Hardman R. A toxicologic review of quantum dots: toxicity depends on physicochemical and environmental factors. Environ. Health Persp. 2006; 114(2):165.
72. Kircher MF, Mahmood U, King RS, Weissleder R, Josephson L. A multimodal nanoparticle for preoperative magnetic resonance imaging and intraoperative optical brain tumor delineation. Cancer Res. 2003; 63(23):8122–8125. [PubMed: 14678964]

73. Santra S, Bagwe RP, Dutta D, et al. Synthesis and characterization of fluorescent, radio-opaque, and paramagnetic silica nanoparticles for multimodal bioimaging applications. Adv. Mat. 2005; 17(18):2165–2169.
74. Park JW. Liposome-based drug delivery in breast cancer treatment. Breast Cancer Res. 2002; 4(3): 95–99. [PubMed: 12052251]
75. Noble C, Krauze M, Drummond D, et al. Novel nanoliposomal CPT-11 infused by convection-enhanced delivery in intracranial tumors: pharmacology and efficacy. Cancer Res. 2006; 66(5): 2801. [PubMed: 16510602]
76. Otsuka H, Nagasaki Y, Kataoka K. PEGylated nanoparticles for biological and pharmaceutical applications. Adv. Drug Deliv. Rev. 2003; 55(3):403–419. [PubMed: 12628324]
77. Davis M. Nanoparticle therapeutics: an emerging treatment modality for cancer. Nat. Rev. Drug Discov. 2008; 7(9):771–782. [PubMed: 18758474]
78. He X, Wang K, Cheng Z. *In vivo* near-infrared fluorescence imaging of cancer with nanoparticle-based probes. Wiley Interdiscip. Rev. Nanomed. Nanobiotechnol. 2010; 2(4):349–366. [PubMed: 20564463]
79. Rafat M, Cleroux CA, Fong WG, et al. PEG–PLA microparticles for encapsulation and delivery of Tat-EGFP to retinal cells. Biomaterials. 1998; 31(12):3414–3421. [PubMed: 20149443]
80. Hu Y, Xie J, Tong YW, Wang CH. Effect of PEG conformation and particle size on the cellular uptake efficiency of nanoparticles with the HepG2 cells. J. Control. Release. 2007; 118(1):7–17. [PubMed: 17241684]
81. Prego C, Torres D, Fernandez-Megia E, et al. Chitosan-PEG nanocapsules as new carriers for oral peptide delivery. Effect of chitosan PEGylation degree. J. Control. Release. 2006; 111(3):299–308. [PubMed: 16481062]
82. Tang BC, Dawson M, Lai SK, et al. Biodegradable polymer nanoparticles that rapidly penetrate the human mucus barrier. Proc. Natl Acad. Sci. USA. 2009; 106(46):19268–19273. [PubMed: 19901335]
83. Malek A, Merkel O, Fink L, et al. *In vivo* pharmacokinetics, tissue distribution and underlying mechanisms of various PEI(-PEG)/siRNA complexes. Toxicol. Appl. Pharmacol. 2009; 236(1): 97–108. [PubMed: 19371615]
84. Santel A, Aleku M, Keil O, et al. A novel siRNA-lipoplex technology for RNA interference in the mouse vascular endothelium. Gene Ther. 2006; 13(16):1222–1234. [PubMed: 16625243]
85. Hirsch L, Stafford R, Bankson J, et al. Nanoshell-mediated near-infrared thermal therapy of tumors under magnetic resonance guidance. Proc. Natl Acad. Sci. USA. 2003; 100(23):13549. [PubMed: 14597719]
86. Koole R, van Schooneveld MM, Hilhorst J, et al. Paramagnetic lipid-coated silica nanoparticles with a fluorescent quantum dot core: a new contrast agent platform for multimodality imaging. Bioconjug. Chem. 2008; 19(12):2471–2479. [PubMed: 19035793]
87. Boyer JC, Manseau MP, Murray JI, van Veggel FC. Surface modification of upconverting NaYF4 nanoparticles with PEG-phosphate ligands for NIR (800 nm) biolabeling within the biological window. Langmuir. 2010; 26(2):1157–1164. [PubMed: 19810725]
88. Munk, P.; Aminabhavi, TM. Introduction to Macromolecular Science. Wiley; NY, USA: 2002.
89. Degennes PG. Polymers at an interface – a simplified view. Adv. Colloid Interface Sci. 1987; 27(3–4):189–209.
90. Degennes PG. Conformations of polymers attached to an interface. Macromolecules. 1980; 13(5): 1069–1075.
91. Levin CS, Bishnoi SW, Grady NK, Halas NJ. Determining the conformation of thiolated poly(ethylene glycol) on Au nanoshells by surface-enhanced Raman scattering spectroscopic assay. Anal. Chem. 2006; 78(10):3277–3281. [PubMed: 16689527]
92. Moghimi S, Szebeni J. Stealth liposomes and long circulating nanoparticles: critical issues in pharmacokinetics, opsonization and protein-binding properties. Progress Lipid Res. 2003; 42(6): 463–478.
93. Mori A, Klibanov A, Torchilin V, Huang L. Influence of the steric barrier activity of amphipathic poly(ethyleneglycol) and ganglioside GM1 on the circulation time of liposomes and on the target binding of immunoliposomes *in vivo*. FEBS Lett. 1991; 284(2):263–266. [PubMed: 2060647]

94. Daou TJ, Li L, Reiss P, Josserand V, Texier I. Effect of poly(ethylene glycol) length on the *in vivo* behavior of coated quantum dots. Langmuir. 2009; 25(5):3040–3044. [PubMed: 19437711]
95. Choi HS, Ipe BI, Misra P, et al. Tissue- and organ-selective biodistribution of NIR fluorescent quantum dots. Nano Lett. 2009; 9(6):2354–2359. [PubMed: 19422261]
96. Ballou B, Lagerholm BC, Ernst LA, Bruchez MP, Waggoner AS. Noninvasive imaging of quantum dots in mice. Bioconjug. Chem. 2004; 15(1):79–86. [PubMed: 14733586]
97. Lin H-H, Cheng Y-L. *In-situ* thermoreversible gelation of block and star copolymers of poly(ethylene glycol) and poly(*N*-isopropylacrylamide) of varying architectures. Macromolecules. 2001; 34(11):3710–3715.
98. Prencipe G, Tabakman SM, Welsher K, et al. PEG branched polymer for functionalization of nanomaterials with ultralong blood circulation. J. Am. Chem. Soc. 2009; 131(13):4783–4787. [PubMed: 19173646]
99. Yoshimoto K, Hirase T, Nemoto S, Hatta T, Nagasaki Y. Facile construction of sulfanyl-terminated poly(ethylene glycol)-brushed layer on a gold surface for protein immobilization by the combined use of sulfanyl-ended telechelic and semitelechelic poly(ethylene glycol)s. Langmuir. 2008; 24(17):9623–9629. [PubMed: 18666758]
100. Ostuni E, Chapman RG, Holmlin RE, Takayama S, Whitesides GM. A survey of structure–property relationships of surfaces that resist the adsorption of protein. Langmuir. 2001; 17(18): 5605–5620.
101. Prime K, Whitesides G. Self-assembled organic monolayers: model systems for studying adsorption of proteins at surfaces. Science. 1991; 252(5009):1164–1167.
102. Zalipsky S. Functionalized poly(ethylene glycol) for preparation of biologically relevant conjugates. Bioconjug. Chem. 1995; 6(2):150–165. [PubMed: 7599259]
103. Kairdolf BA, Mancini MC, Smith AM, Nie S. Minimizing nonspecific cellular binding of quantum dots with hydroxyl-derivatized surface coatings. Anal. Chem. 2008; 80(8):3029–3034. [PubMed: 18324840]
104. Parrish B, Breitenkamp RB, Emrick T. PEG- and peptide-grafted aliphatic polyesters by click chemistry. J. Am. Chem. Soc. 2005; 127(20):7404–7410. [PubMed: 15898789]
105. Collard DM, Fox MA. Use of electroactive thiols to study the formation and exchange of alkanethiol monolayers on gold. Langmuir. 1991; 7(6):1192–1197.
106. Mei BC, Susumu K, Medintz IL, et al. Modular poly(ethylene glycol) ligands for biocompatible semiconductor and gold nanocrystals with extended pH and ionic stability. J. Mat. Chem. 2008; 18(41):4949–4958.
107. Liu Z, Davis C, Cai W, et al. Circulation and long-term fate of functionalized, biocompatible single-walled carbon nanotubes in mice probed by Raman spectroscopy. Proc. Natl Acad. Sci. USA. 2008; 105(5):1410. [PubMed: 18230737]
108. Hong Y, Shin D, Cho S, Uhm H. Surface transformation of carbon nanotube powder into super-hydrophobic and measurement of wettability. Chem. Phys. Lett. 2006; 427(4–6):390–393.
109. Chan JM, Zhang LF, Yuet KP, et al. PLGA-lecithin-PEG core-shell nanoparticles for controlled drug delivery. Biomaterials. 2009; 30(8):1627–1634. [PubMed: 19111339]
110. Huang HC, Chang PY, Chang K, et al. Formulation of novel lipid-coated magnetic nanoparticles as the probe for *in vivo* imaging. J. Biomed. Sci. 2009; 16(10)
111. Dubertret B, Skourides P, Norris DJ, et al. *In vivo* imaging of quantum dots encapsulated in phospholipid micelles. Science. 2002; 298(5599):1759–1762. [PubMed: 12459582]
112. Goren D, Horowitz A, Tzemach D, et al. Nuclear delivery of doxorubicin via folate-targeted liposomes with bypass of multidrug-resistance efflux pump. Clin. Cancer Res. 2000; 6(5):1949. [PubMed: 10815920]
113. Hoarau D, Delmas P, David S, Roux E, Leroux JC. Novel long-circulating lipid nanocapsules. Pharmaceut. Res. 2004; 21(10):1783–1789.
114. Brown, W. Dynamic Light Scattering: the Method and Some Applications. Oxford University Press; USA: 1993.
115. Garbuzenko O, Barenholz Y, Priev A. Effect of grafted PEG on liposome size and on compressibility and packing of lipid bilayer. Chem. Phys. Lipids. 2005; 135(2):117–129. [PubMed: 15921973]

116. Steinmetz NF, Hong V, Spoerke ED, et al. Buckyballs meet viral nanoparticles: candidates for biomedicine. J. Am. Chem. Soc. 2009; 131(47):17093–17095. [PubMed: 19904938]
117. Butterworth M, Illum L, Davis S. Preparation of ultrafine silica-and PEG-coated magnetite particles. Colloids Surfaces A: Physicochem. Engin. Asp. 2001; 179(1):93–102.
118. Garcia-Fuentes M, Torres D, Martín-Pastor M, Alonso M. Application of NMR spectroscopy to the characterization of PEG-stabilized lipid nanoparticles. Langmuir. 2004; 20(20):8839–8845. [PubMed: 15379515]
119. Duncanson W, Figa M, Hallock K, et al. Targeted binding of PLA microparticles with lipid-PEG-tethered ligands. Biomaterials. 2007; 28(33):4991–4999. [PubMed: 17707503]
120. Jokerst JV, Miao Z, Zavaleta C, Cheng Z, Gambhir SS. Affibody functionalized gold-silica nanoparticles for Raman molecular imaging of the epidermal growth factor receptor. Small. 2011; 7(5):625–633. [PubMed: 21302357]
121. Demers L, Mirkin C, Mucic R, et al. A fluorescence-based method for determining the surface coverage and hybridization efficiency of thiol-capped oligonucleotides bound to gold thin films and nanoparticles. Anal. Chem. 2000; 72(22):5535–5541. [PubMed: 11101228]
122. Eck W, Craig G, Sigdel A, et al. PEGylated gold nanoparticles conjugated to monoclonal F19 antibodies as targeted labeling agents for human pancreatic carcinoma tissue. ACS Nano. 2008; 2(11):2263–2272. [PubMed: 19206392]
123. Ehrlich GK, Michel H, Chokshi HP, Malick AW. Affinity purification and characterization of an anti-PEG IgM. J. Mol. Recognit. 2009; 22(2):99–103. [PubMed: 18850671]
124. Zabaleta V, Campanero M, Irache J. An HPLC with evaporative light scattering detection method for the quantification of PEGs and Gantrez in PEGylated nanoparticles. J. Pharmaceut. Biomed. Anal. 2007; 44(5):1072–1078.
125. Boddy AV, Plummer ER, Todd R, et al. A Phase I and pharmacokinetic study of paclitaxel poliglumex (XYOTAX), investigating both 3-weekly and 2-weekly schedules. Clin. Cancer Res. 2005; 11(21):7834–7840. [PubMed: 16278406]
126. Nagasaki Y, Kobayashi H, Katsuyama Y, Jomura T, Sakura T. Enhanced immunoresponse of antibody/mixed-PEG co-immobilized surface construction of high-performance immunomagnetic ELISA system. J. Colloid Interface Sci. 2007; 309(2):524–530. [PubMed: 17368469]
127. Farokhzad OC, Cheng J, Teply BA, et al. Targeted nanoparticle-aptamer bioconjugates for cancer chemotherapy *in vivo*. Proc. Natl Acad. Sci. USA. 2006; 103(16):6315–6320. [PubMed: 16606824]
128. Winter P, Morawski A, Caruthers S, et al. Molecular imaging of angiogenesis in early-stage atherosclerosis with $\{\alpha\}_V\{\beta\}_3$-integrin-targeted nanoparticles. Circulation. 2003; 108(18):2270. [PubMed: 14557370]
129. DeNardo S, DeNardo G, Miers L, et al. Development of tumor targeting bioprobes (^{111}In-chimeric L6 monoclonal antibody nanoparticles) for alternating magnetic field cancer therapy. Clin. Cancer Res. 2005; 11(19):7087S–7092S. [PubMed: 16203807]
130. Banerjee R, Tyagi P, Li S, Huang L. Anisamide targeted stealth liposomes: a potent carrier for targeting doxorubicin to human prostate cancer cells. Int. J. Cancer. 2004; 112(4):693–700. [PubMed: 15382053]
131. Smith BR, Cheng Z, De A, et al. Real-time intravital imaging of RGD-quantum dot binding to luminal endothelium in mouse tumor neovasculature. Nano Lett. 2008; 8(9):2599–2606. [PubMed: 18386933]
132. Sonvico F, Mornet S, Vasseur S, et al. Folate-conjugated iron oxide nanoparticles for solid tumor targeting as potential specific magnetic hyperthermia mediators: synthesis, physicochemical characterization, and *in vitro* experiments. Bioconjug Chem. 2005; 16(5):1181–1188. [PubMed: 16173796]
133. Lee A, Wang Y, Ye W, et al. Efficient intracellular delivery of functional proteins using cationic polymer core/shell nanoparticles. Biomaterials. 2008; 29(9):1224–1232. [PubMed: 18078986]
134. Cheng J, Teply BA, Sherifi I, et al. Formulation of functionalized PLGA-PEG nanoparticles for *in vivo* targeted drug delivery. Biomaterials. 2007; 28(5):869–876. [PubMed: 17055572]

135. Hackel B, Kapila A, Dane Wittrup K. Picomolar affinity fibronectin domains engineered utilizing loop length diversity, recursive mutagenesis, and loop shuffling. J. Mol. Biol. 2008; 381(5): 1238–1252. [PubMed: 18602401]

136. Yang LL, Peng XH, Wang YA, et al. Receptor-targeted nanoparticles for *in vivo* imaging of breast cancer. Clin. Cancer Res. 2009; 15(14):4722–4732. [PubMed: 19584158]

137. Cai W, Chen X. Multimodality molecular imaging of tumor angiogenesis. J. Nucl. Med. 2008; 49(Suppl. 2):113S–28S. [PubMed: 18523069]

138. Nagasaki Y, Kobayashi H, Katsuyama Y, Jomura T, Sakura T. Enhanced immunoresponse of antibody/mixed-PEG co-immobilized surface construction of high-performance immunomagnetic ELISA system. J. Colloid Interface Sci. 2007; 309(2):524–530. [PubMed: 17368469]

139. Wang M, Lowik D, Miller AD, Thanou M. Targeting the urokinase plasminogen activator receptor with synthetic self-assembly nanoparticles. Bioconjugate Chem. 2009; 20(1):32–40.

140. Mustapa MFM, Grosse SM, Kudsiova L, et al. stabilized integrin-targeting ternary LPD (lipopolyplex) vectors for gene delivery designed to disassemble within the target cell. Bioconjugate Chem. 2009; 20(3):518–532.

141. Patil YB, Toti US, Khdair A, Ma L, Panyam J. Single-step surface functionalization of polymeric nanoparticles for targeted drug delivery. Biomaterials. 2009; 30(5):859–866. [PubMed: 19019427]

142. Caliceti P, Veronese F. Pharmacokinetic and biodistribution properties of poly (ethylene glycol)-protein conjugates. Adv. Drug Delivery Rev. 2003; 55(10):1261–1277.

143. Ishida T, Ichihara M, Wang X, Kiwada H. Spleen plays an important role in the induction of accelerated blood clearance of PEGylated liposomes. J. Control. Release. 2006; 115(3):243–250. [PubMed: 17011060]

144. Zhao X, Bagwe R, Tan W. Development of organic-dye-doped silica nanoparticles in a reverse microemulsion. Adv. Mat. 2004; 16(2):173–176.

145. Mitra S, Gaur U, Ghosh P, Maitra A. Tumour targeted delivery of encapsulated dextran-doxorubicin conjugate using chitosan nanoparticles as carrier. J. Control. Release. 2001; 74(1–3): 317–323. [PubMed: 11489513]

146. Lin Y, Böker A, He J, et al. Self-directed self-assembly of nanoparticle/copolymer mixtures. Nature. 2005; 434(7029):55–59. [PubMed: 15744296]

147. Smith A, Duan H, Rhyner M, Ruan G, Nie S. A systematic examination of surface coatings on the optical and chemical properties of semiconductor quantum dots. Phys. Chem. Chem. Phys. 2006; 8(33):3895–3903. [PubMed: 19817050]

148. Scott RW, Wilson OM, Crooks RM. Synthesis, characterization, and applications of dendrimer-encapsulated nanoparticles. J. Phys. Chem. B. 2005; 109(2):692–704. [PubMed: 16866429]

149. Mulder W, Strijkers G, Habets J, et al. MR molecular imaging and fluorescence microscopy for identification of activated tumor endothelium using a bimodal lipidic nanoparticle. FASEB J. 2005; 19:2008–2010. [PubMed: 16204353]

150. Zalipsky S, Qazen M, Walker J II, et al. New detachable poly(ethylene glycol) conjugates: cysteine-cleavable lipopolymers regenerating natural phospholipid, diacyl phosphatidylethanolamine. Bioconjugate Chem. 1999; 10(5):703–707.

151. Takae S, Miyata K, Oba M, et al. PEG-detachable polyplex micelles based on disulfide-linked block catiomers as bioresponsive nonviral gene vectors. J. Am. Chem. Soc. 2008; 130(18):6001–6009. [PubMed: 18396871]

152. Choi MR, Stanton-Maxey KJ, Stanley JK, et al. A cellular Trojan Horse for delivery of therapeutic nanoparticles into tumors. Nano Lett. 2007; 7(12):3759–3765. [PubMed: 17979310]

153. Akin D, Sturgis J, Ragheb K, et al. Bacteria-mediated delivery of nanoparticles and cargo into cells. Nat. Nanotechnol. 2007; 2(7):441–449. [PubMed: 18654330]

154. Schmaljohann D. Thermo- and pH-responsive polymers in drug delivery. Adv. Drug Deliv. Rev. 2006; 58(15):1655–1670. [PubMed: 17125884]

155. Mok H, Veiseh O, Fang C, et al. pH-sensitive siRNA nanovector for targeted gene silencing and cytotoxic effect in cancer cells. Mol. Pharm. 1930; 7(6):1930–1939. [PubMed: 20722417]

156. Shenoy D, Little S, Langer R, Amiji M. Poly (ethylene oxide)-modified poly (-amino ester) nanoparticles as a pH-sensitive system for tumor-targeted delivery of hydrophobic drugs. 1. *In vitro* evaluations. Mol. Pharm. 2005; 2(5):357–366. [PubMed: 16196488]

Executive summary

- The body's reticuloendothelial system sweeps foreign nanoparticles (NPs) out of the circulation before reaching the intended target. Coating the NP with polyethylene glycol (PEG) can reduce this phenomenon and result in longer circulation times.
- Longer circulation times can result from longer PEG chains, denser (heavier coating on NP surface) PEG chains or branched PEG chains.
- The terminus of the PEG chain influences charge and stability. Methoxy-capped chains are most effective at preventing recognition by the reticuloendothelial system. Targeting ligands bound to the PEG chain terminus can increase uptake at the target.
- The amount of PEG on a NP is measured by optical and chromatographic methods or gravimetric analysis. The NMR peak is approximately 3.7 parts per million.
- Alternatives to PEG include saccharides, copolymers and lipids. Cells and bacteria have been used in lieu of NPs as delivery vehicles.

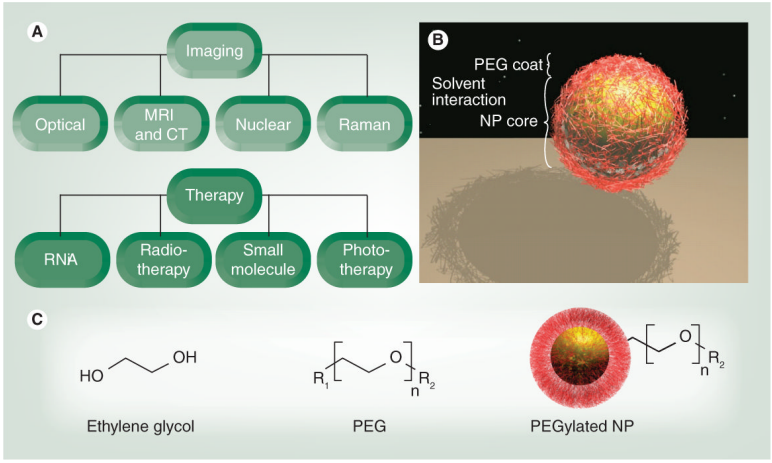

Figure 1. Nanoparticle applications of polyethylene glycol

(A) The use of NPs in imaging involves different modalities, including optical and radionuclide techniques. In therapy, diverse NPs carry a range of payloads, including radiotherapy, nucleic acids and small molecules. **(B)** PEGylated NP, indicating a firmer metallic or polymeric core (yellow) with a surrounding cloud of flexible PEG chains (red). **(C)** Monomers of ethylene glycol are polymerized into PEG for NP coating. PEG contains the linkage group (R_1) and a terminus that interacts with solvent (R_2).

NP: Nanoparticle; PEG: Polyethylene glycol.

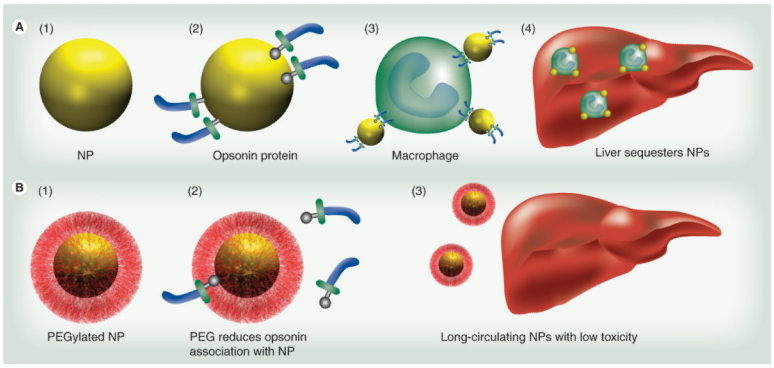

Figure 2. Polyethylene glycol prevents uptake by the reticuloendothelial system

(A) Nanoparticles **(A1)** are coated with opsonin proteins **(A2)** and associate with macrophages **(A3)** for transit to the liver **(A4)**. Macrophages stationary in the liver, known as Kupffer cells, also participate in nanoparticle scavenging. **(B)** Nanoparticles coated with PEG coating **(B1)** prevents this opsonization **(B2)**, resulting in decreased liver accumulation **(B3)** and increased availability of the NP for imaging or therapy.

NP: Nanoparticle; PEG: Polyethylene glycol.

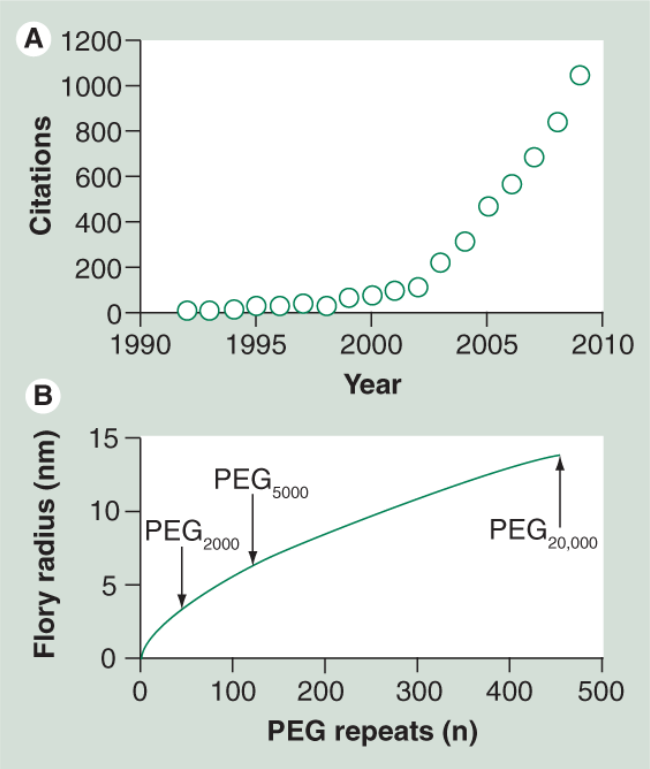

Figure 3. Polyethylene glycol background

(A) The number of literature citations for `nanoparticle + PEG' as determined by Chemical Abstract Services indicates a progressive increase in the last decade. **(B)** The Flory radius of the PEG coil increases as a function of the number of monomers (n); see Equation 1.
PEG: Polyethylene glycol.

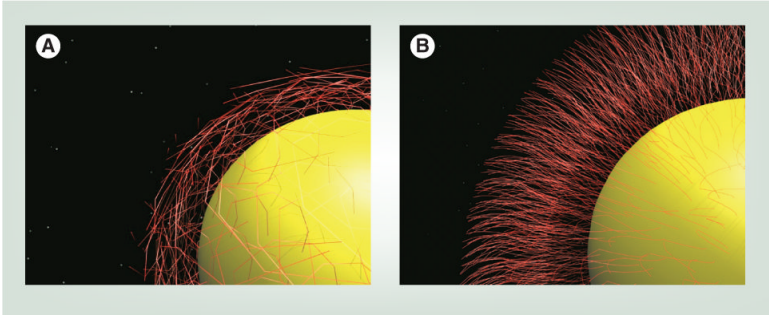

Figure 4. Gold spherical nanoparticle with two types of polyethylene glycol modifications
Polyethylene glycol orientations on the nanoparticle surface include **(A)** low-density mushroom configurations and **(B)** high-density brush-type arrangements.

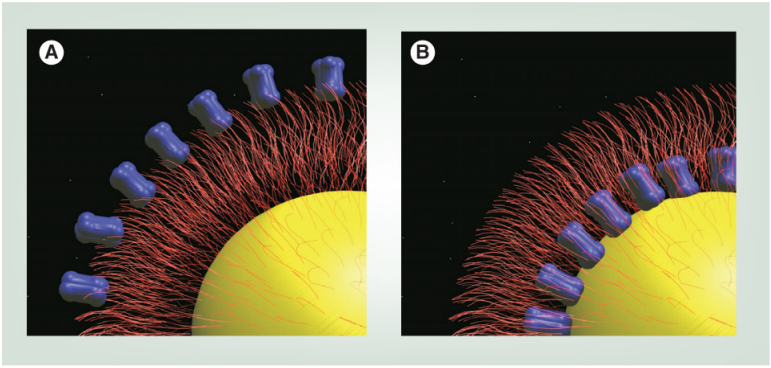

Figure 5. Increased affinity for targeted nanoparticles

(A) In targeted nanoparticles, the ligand (blue) may either be localized on the distal end of the polyethylene glycol chain or **(B)** at the nanoparticle surface. A wide variety of ligand and nanoparticle combinations have been reported, including the examples in this article. See Table 4.

Table 1

PEGylation strategies used to combine ethylene glycol repeats with nanoparticles.

Application	Nanoparticle	Nanoparticle size (nm)	R_1	R_2	n	Molecular weight (g/mol)	Ref.
Imaging	Gold	13	SH	MeO	113	5000	[57]
Imaging	Gold	15	DHLA	MeO, NH_2, COOH	14	600	[106]
Imaging	Silica quantum dots	34.3	DSPE (lipid; 1,2-distearoyl-*sn*-glycero-3-phosphoethanolamine)	MeO	45	2000	[86]
Imaging	$NaYF_4$	17	Phosphate	MeO	17,45	750, 2000	[87]
Imaging	Magnetic silica	60	$Si(OCH_3)_3$	MeO	6–9	300–400	[64]
Magnetic resonance contrast	Fe_3O_4	9	Dopamine	COOH	14–455	600–20,000	[53]
Drug delivery	Poly(lactic-co-glycolic acid)/ polyethylene glycol	70–250	NH_2	COOH	77	3400	[127]
Drug delivery	Gold	3,6.5	C_{11}-SH	OH	4	160	[14]
Drug delivery	Poly(hexadecylcyanoacrylate)	150	Cyanoacetate	MeO	45	2000	[21]
Phototherapy	Gold nanorod	13 ×47	SH	MeO	113	5000	[62]
Photosensitizer	Cowpea mosaic virus Fullerene	30 (cowpea mosaic virus) 1 (fullerene)	NH_2	Alkyne	23	1000	[116]

The polyethylene glycol system has both units for annealing to nanoparticle surface (indicated by R_1) and units to interface with the solvent (R_2) (Figure 1). The length of polyethylene glycol is influenced by the number of monomers (n). Here, the variety of PEGylation strategies is emphasized, including diverse nanoparticle and polyethylene glycol types, as well as conjugation type. DHLA: Dihydrolipoic acid.

Table 2

Approaches to measuring the polyethylene glycol density on the nanoparticle surface.

Technique	NP type	NP size (radius; nm)	PEG molecular weight (kDa)	Footprint (nm^2)	Coverage ($pmol/cm^2$)	PEG/NP	Ref.
Raman	Gold nanoshell	107	2000	3.6	47 ± 21	40,500	[91]
Raman	Gold nanoshell	107	5000	10.8	15.3 ± 8	13,300	[91]
Gel electrophoresis	Cowpea mosaic virus	15	1000 or 2000	91–135	1.2–1.8	21–31	[116]
Thermogravimetry	Fe_3O_4	15–20	200–5000	1–3	57–128	970–3900	[117]
Thermogravimetry	Gold NP	1.4–2.6	5000	0.21–0.35	655–1005	98–506	[57]
NMR	Microparticle	250–1000	2000 or 5000	4.8 (5000) 1.8(2000)	34–90	(1.–12.5) $\times 10^6$	[119]
NMR	Tripalmitin	126–173	1760	0.25–1	83–540	99,000–550,000	[118]

A variety of methods have been proposed to determine PEG:NP loading levels. Higher loading levels provide more dense coverage and smaller PEG footprints (PEG/NP surface area). NP: Nanoparticle; PEG: Polyethylene glycol; PLGA: Poly(lactic-co-glycolic acid).

Table 3

Circulation times in mouse for representative nanoparticles.

NP type	Size (nm)	PEG	PEG molecular weight (kDa)	$t_{1/2}$ (h)	Ref.
QD655	15	mPEG; linear	5000	~1	[96]
Fluorescent silica	80	mPEG; linear	500	3	[63]
Single-walled carbon nanotube	~100	mPEG; linear	5000	5.4	[107]
Poly(hexadecylcyanoacrylate)	150	mPEG; linear	2000	~6	[21]
Nanorods	13 × 47	mPEG; linear	5000	17	[62]
Single-walled carbon nanotube	~100	PLGA–PEG; branch	5000	22	[19]

Well-PEGylated NPs have a half-life approaching 1 day.

mPEG: Methoxy-polyethylene glycol; NP: Nanoparticle; PEG: Polyethylene glycol; PLGA: Poly(lactic-co-glycolic acid); QD: Quantum dot.

Table 4

Ligand and nanoparticle combinations reported to increase affinity for targeted nanoparticles.

Nanoparticle	Ligand	Target	Sample	Ligand location	Ref.
Quantum dots	RGD	Integrins	U87MG tumor	PEG	[131]
Iron oxide	Folate	Folate receptor	KB 3-1 cells	PEG	[132]
Liposome	Anisamide	σ receptor	DU-145 cells	PEG	[130]
Liposome	Folate	Folate receptor	M109 cells	PEG	[112]
PLGA–PEG	Aptamer	Prostate-specific membrane antigen	LnCaP cells	PEG	[127]
Fe_2O_3	Antibody	α-feto protein	Buffer; cell lysate	Surface	[126]

See Figure 5 *for illustrations of targeted nanoparticles*.

PEG: Polyethylene glycol; PLGA: Poly(lactic-co-glycolic acid).